

$B \rightarrow K^* \ell \ell$ Standard Model contributions – Zooming in on high q^2

G. Hiller

Institut für Physik, Technische Universität Dortmund, D-44221 Dortmund, Germany

To further precision studies with $B \rightarrow K^{(*)} \ell \ell$ decays in the high- q^2 window uncertainties related to the operator product expansion (OPE) need to be scrutinized. How well can the OPE describe $B \rightarrow K^*(\rightarrow K\pi) \ell \ell$ angular distributions for a given binning in view of the local charm resonance structure? We present a data-driven method to access this quantitatively. Our analysis suggests that the bins which are near the kinematic endpoint are best described by the OPE and should be pursued for precision studies. At the same time measurements with finer binning help controlling the uncertainties.

1 Introduction

Rare decays of B -mesons into leptons are key modes to test the Standard Model (SM) and look for New Physics¹. In particular $B \rightarrow K^*(\rightarrow K\pi) \mu \mu$ decays have received high and growing interest due to their sensitivity to flavor physics in and beyond the SM and the feasibility for precision studies at hadron and e^+e^- -colliders. Recent data from the LHC cover several thousands of events into muons, and include various angular distributions^{2 3 4}. There are great prospects for Run II and future machines⁵, including various other final lepton species (e, τ, ν).

$B \rightarrow K^{(*)} \ell \ell$ decays are described by $1/m_b$ -methods, in both the region of low dilepton mass squared q^2 , below the J/Ψ , and the high- q^2 region above the Ψ' . In the latter is $q^2 \sim \mathcal{O}(m_b^2)$ and an operator product expansion (OPE) applies⁶. Among its benefits is the good convergence, power corrections linear in $1/m_b$ receive additional parametric suppression, and the resulting universality of short-distance coefficients $C^{L,R}$ in the longitudinal (0), parallel (\parallel) and perpendicular (\perp) transversity amplitudes⁷

$$A_j^{L,R}(q^2) \simeq \mathcal{C}^{L,R}(q^2) f_j(q^2) + \mathcal{O}(1/m_b), \quad j = 0, \parallel, \perp. \quad (1)$$

Here,

$$\mathcal{C}^{L,R}(q^2) = \mathcal{C}_9^{\text{eff}}(q^2) \mp \mathcal{C}_{10} + \kappa \frac{2m_b m_B}{q^2} \mathcal{C}_7^{\text{eff}}(q^2), \quad (2)$$

where \mathcal{C}_i are the Wilson coefficients of the radiative and semileptonic operators, respectively,

$$\mathcal{O}_7 = \frac{e}{16\pi^2} m_b \bar{s} \sigma^{\mu\nu} P_R b F_{\mu\nu}, \quad \mathcal{O}_9 = \frac{e^2}{16\pi^2} (\bar{s} \gamma^\mu P_L b) (\bar{\ell} \gamma_\mu \ell), \quad \mathcal{O}_{10} = \frac{e^2}{16\pi^2} (\bar{s} \gamma^\mu P_L b) (\bar{\ell} \gamma_\mu \gamma_5 \ell), \quad (3)$$

and the f_j are transversity form factors. The effective coefficients $\mathcal{C}_{7,9}^{\text{eff}}$ equal $\mathcal{C}_{7,9}$ up to contributions from 4-quark operators. Including right-handed currents from BSM physics, the universality of amplitudes Eq. (1) breaks down to a partial one between the (0) and (\parallel) amplitudes.

As the OPE relies on duality⁸ its performance depends on bin size and location. In particular, too small bin intervals will start to resolve local resonance structure induced by charm contributions $B \rightarrow K^*(c\bar{c}) \rightarrow K^* \ell \ell$, shown in Figure 1, and limit the accuracy of the OPE predictions

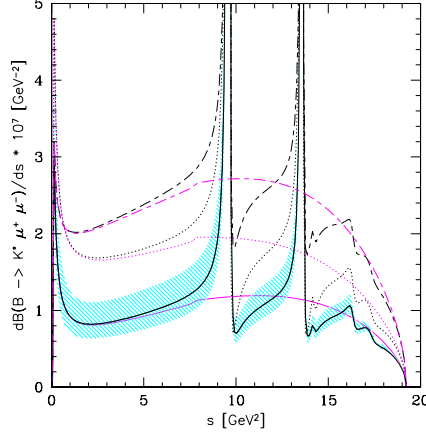


Figure 1 – The differential branching fraction $d\mathcal{B}/dq^2(B \rightarrow K^* \mu \mu)$ in the SM (solid curves) and BSM scenarios (dotted and dash-dotted curves). Black curves include resonances based on the KS-approach¹⁰ while the magenta ones are short-distance only. The high- q^2 region begins above the ψ' -peak, note the wiggles. Figure taken from⁹.

at high q^2 . As we can't tell this from within the OPE, we employ a local model parametrization as a test-case against the OPE.

2 The high- q^2 region locally

Charm contributions are electromagnetically induced and modify the operator with vector coupling to leptons, \mathcal{O}_9 . The OPE covers such effects; they are part of the effective coefficient $\mathcal{C}_9^{\text{eff}}$ and read, up to terms of order α_s and neglecting contributions from non-charm penguin operators,

$$\mathcal{C}_9^{\text{eff}}(q^2) = \mathcal{C}_9 + h(q^2, m_c^2) \left[\frac{4}{3} \mathcal{C}_1 + \mathcal{C}_2 + 6\mathcal{C}_3 + 60\mathcal{C}_5 \right] + \dots \quad (4)$$

The loop function $h(q^2, m_c^2)$ is obtained perturbatively from insertions of $\bar{s}b\bar{c}c$ -type operators and is smooth in the high- q^2 region⁶.

In Figure 2 the "short-distance-free" observables S_3, S_4 and F_L in the OPE (red curves and boxes with form factors from¹¹) are compared to data (black, converted to theory conventions), zooming in from 2 GeV^2 bins (upper plots) to 1 GeV^2 bins (lower plots). Quite generally one expects from the R -ratio¹² an onset of resonance structure with this resolution. Indeed the alternating patterns in the 1 GeV^2 bins may be hinting at resonances, however, due to the limited experimental precision, one cannot draw firm conclusions presently. Plots with further observables, S_5, A_{FB} and $d\mathcal{B}/dq^2$, are given in¹³.

Furthermore, the data have to meet the endpoint relations at $q_{\text{max}}^2 = (m_B - m_{K^*})^2$, which follow from Lorentz-invariance and hold irrespective of the underlying electroweak model¹⁴

$$F_L(q_{\text{max}}^2) = 1/3, \quad S_3(q_{\text{max}}^2) = -1/4, \quad S_4(q_{\text{max}}^2) = 1/4, \quad S_{5,6,7,8,9}(q_{\text{max}}^2) = 0. \quad (5)$$

In particular with 1 GeV^2 bins data on $S_{3,4,5}$ are presently in mild conflict with the endpoint relations. Further data with improved precision is required to clarify these points.

To test the accuracy of the OPE for a given binning we employ a model that is able to locally capture resonance effects which show up as "wiggles" in the $B \rightarrow K^* \ell \ell$ distributions. We follow the method of Krüger and Sehgal (KS)¹⁰, which uses e^+e^- -data on the vacuum polarization to describe the charm-loop function as

$$\mathcal{C}_9^{\text{eff}}(q^2)|^{KS} = \mathcal{C}_9 + (3a_2) \eta_c h_c(q^2) + \dots, \quad (6)$$

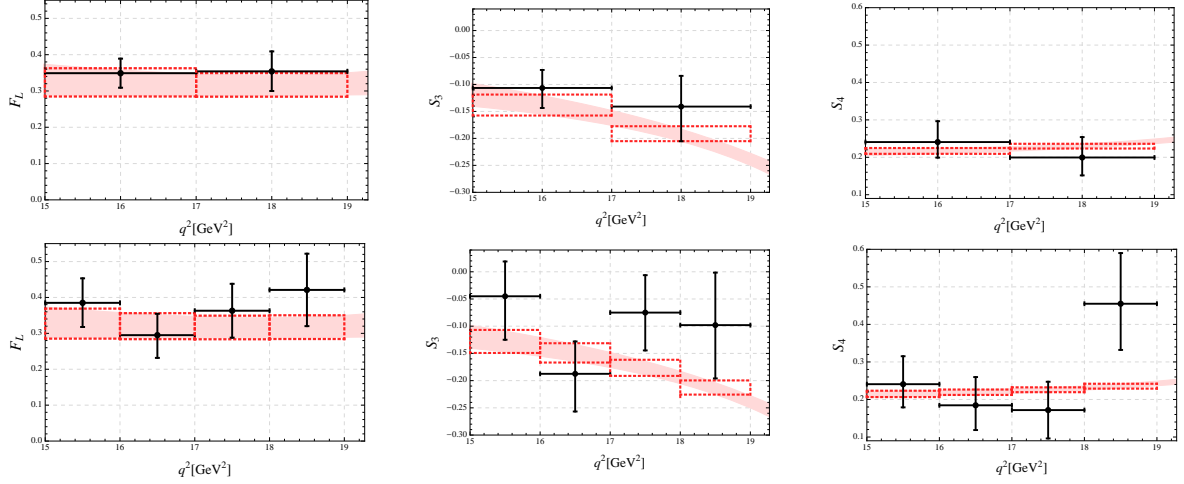


Figure 2 – F_L , S_3 and S_4 in the OPE for 2 GeV^2 bins (upper plots) and 1 GeV^2 bins (lower plots) shown as red boxes versus data (black) from LHCb³. Systematic and statistical uncertainties are added in quadrature. The light-shaded red bands illustrate the OPE for infinitesimal binning. Plots taken from¹³.

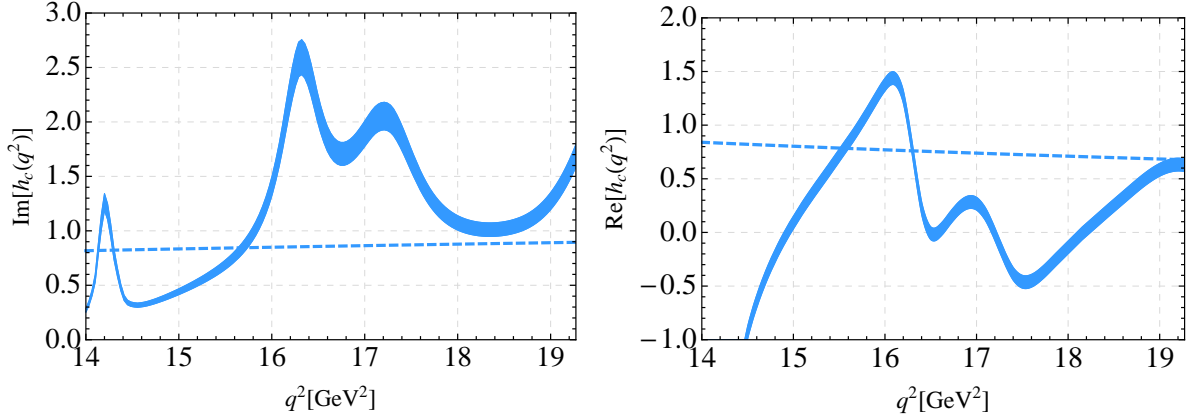


Figure 3 – The charm polarization function $h_c(q^2)$ from $e^+e^- \rightarrow \text{hadrons}$ data (blue 1σ band). The corresponding OPE-contributions, imaginary and real part of $h(q^2, m_c^2)$, are shown by the blue dashed lines. Plots taken from¹³.

where

$$\text{Im } h_c(q^2) = \frac{\pi}{3} R_c(q^2), \quad R_c = \frac{\sigma(e^+e^- \rightarrow c\bar{c})}{\sigma(e^+e^- \rightarrow \mu^+\mu^-)}. \quad (7)$$

The real part of $h_c(q^2)$ is obtained from a dispersion integral. The real and imaginary part of h_c extracted from a fit to BES data¹² can be seen in Figure 3, consistent with¹⁵. a_2 is the same combination of Wilson coefficients that accounts for the perturbative charm-loop

$$a_2 = \frac{1}{3} \left(\frac{4}{3} C_1 + C_2 + 6C_3 + 60C_5 \right). \quad (8)$$

Numerically, to NNLO accuracy at the b -mass scale, $a_2 = 0.2$. (In the operator basis used in earlier works $3a_2$ corresponds to $C^{(0)}$ ⁹.) The factor η_c has been introduced to account for corrections from beyond naive factorization, $\eta_c = 1$. Such effects are expected quite generally as $B \rightarrow K^{(*)}(c\bar{c})$ decays are prominent examples of modes with violent breaking of naive factorization¹⁶, yet a comparison of the factorization formula with measured branching ratios yields $|\eta_{(J/\psi, \Psi(2S)) K^*}| \simeq 0.9 - 1$.

We go beyond the original works¹⁰ and generalize Eq. (6) by introducing transversity-dependent fudge functions $\eta_c(K_j^*, q^2)$ to obtain a model that can fit $B \rightarrow K^* \ell \ell$ distributions

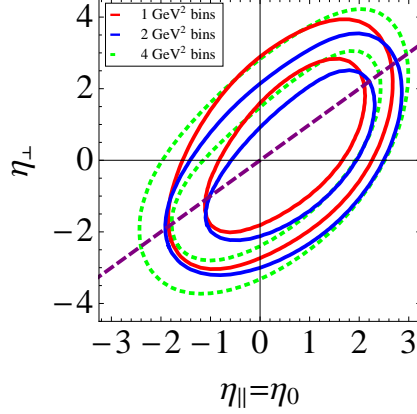


Figure 4 – 1 and 2 σ constraints on $\eta_{\perp}, \eta_{\parallel} = \eta_0$ from $B \rightarrow K^* \mu \mu$ data³ at high q^2 for fixed binning 4 GeV^2 (green, dotted), 2 GeV^2 (blue) and 1 GeV^2 (red) as in Eq. (10). The dashed magenta straight line denotes the universality-limit $\eta_{\perp} = \eta_0 = \eta_{\parallel}$. Plot taken from¹³.

in principle with any precision limited only by input other than that of the resonances, such as perturbative one and form factors. Note that symmetries at the endpoint dictate¹⁴

$$\eta_c(K_0^*, q_{\text{max}}^2) = \eta_c(K_{\parallel}^*, q_{\text{max}}^2), \quad (9)$$

but other than that the functions should be constrained experimentally.

To make progress we use constant η_{\perp} and $\eta_{\parallel} = \eta_0$ to comply with Eq. (9). We define $\eta_j \equiv \eta_c(K_j^*, q^2)$. With improved data one can consider different shapes.

3 Fitting $B \rightarrow K^* \mu \mu$ observables

One benefits from the availability of $B \rightarrow K^*(\rightarrow K\pi)\mu\mu$ data³ in different binings

$$[15 - 19] \text{ GeV}^2, \quad [15 - 17], [17 - 19] \text{ GeV}^2, \quad [15 - 16], \dots, [18 - 19] \text{ GeV}^2 \quad (10)$$

allowing to zoom in with resolution $\Delta q^2 = 4, 2$ and 1 GeV^2 , respectively. As we assume new physics at the electroweak scale and beyond, *a binning-related effect is due to resonances, not New Physics*.

In addition to S_3, S_4 and F_L , in which universal effects drop out, we consider the angular observables $J_{5,\dots,9}$ and the differential branching fraction, $d\mathcal{B}/dq^2$. As these are short-distance dependent, we are forced to perform a joined extraction of η 's and \mathcal{C} 's. We simultaneously fit to $\eta_{\perp}, \eta_{\parallel}$ and New Physics contributions $\delta\mathcal{C}_9, \delta\mathcal{C}_{10}$ for each q^2 -resolution $\Delta q^2 = 4, 2$ and 1 GeV^2 . Results are shown in Figure 4 for the η 's and in Figure 5 for the Wilson coefficients. As presently there are no data on the branching ratio for 1 GeV^2 bins available, we use in the latter analysis the 2 GeV^2 finding⁴. This is not ideal as it certainly blurs the zooming effect, however we chose to keep the branching ratio as an important constraint in the fit. Form factors are taken from lattice QCD¹¹.

From Figure 4 we learn that naive factorization, $\eta_j = 1$, is allowed, but also solutions away from universality, $\eta_{\perp} = \eta_0 = \eta_{\parallel}$, shown by the dashed line. The constraints from the largest q^2 -resolution (green, dotted) are the weakest. The fits are presently consistent with no wiggles, $\eta_j = 0$. However, modulo experimental uncertainties, binning-induced differences hint at the presence of such structure.

Fits to the BSM-coefficients $\delta\mathcal{C}_9, \delta\mathcal{C}_{10}$, see Figure 5, give very similar results for the OPE and the local model, for each Δq^2 -resolution. This implies that at current level of precision, the OPE describes the data sufficiently well as we are not yet fully sensitive to charm resonances.

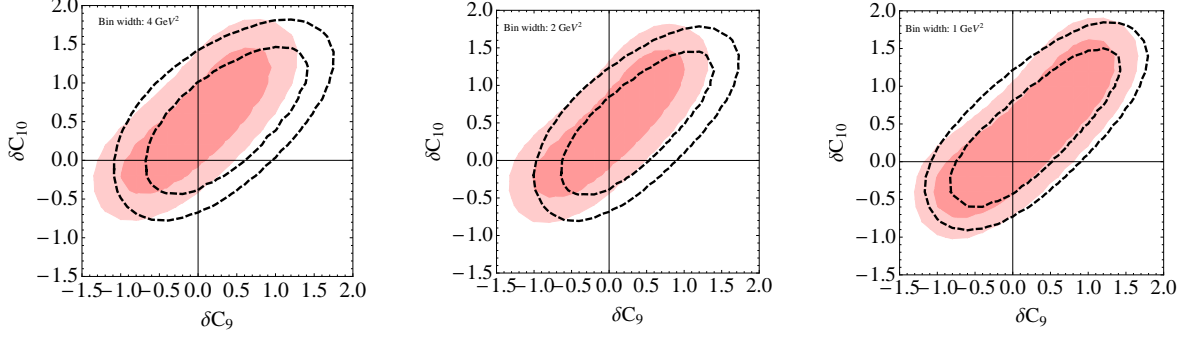


Figure 5 – 1 and 2 σ constraints on $\delta\mathcal{C}_9, \delta\mathcal{C}_{10}$ from $B \rightarrow K^* \mu\mu$ data³ at high q^2 for fixed binning 4 GeV^2 (left), 2 GeV^2 (center) and 1 GeV^2 (right) as in Eq. (10). Red shaded areas (black contours) denote the allowed regions in the OPE (in the KS-approach with $\eta_\perp, \eta_\parallel = \eta_0$ simultaneously fitted). Plots taken from¹³.

Table 1: Ranges of ϵ_k defined in Eq. (11) for different q^2 -bins in GeV^2 and 1σ ranges of parameters $\eta_{\perp, \parallel}, \mathcal{C}_{9,10}$.

| | 15 – 19 | 15 – 17 | 17 – 19 | 15 – 16 | 16 – 17 | 17 – 18 | 18 – 19 |
|-----------------|--------------|--------------|--------------|--------------|--------------|--------------|--------------|
| ϵ_1 | (0.85, 1.16) | (0.81, 1.30) | (0.87, 1.03) | (0.76, 1.20) | (0.84, 1.38) | (0.84, 1.03) | (0.86, 1.05) |
| ϵ_2 | (0.82, 1.0) | (0.74, 1.13) | (0.85, 0.91) | (0.71, 1.17) | (0.78, 1.08) | (0.76, 0.95) | (0.84, 0.97) |
| ϵ_{12} | (0.86, 1.05) | (0.87, 1.05) | (0.84, 1.05) | (0.95, 1.06) | (0.78, 1.05) | (0.75, 1.05) | (0.93, 1.05) |

The plots also show that the SM is allowed but also sizable BSM effects, in agreement with the plain low recoil analysis of¹⁷. An analogous fit to $\eta_\perp, \eta_\parallel$ and the Wilson coefficients of the chirality-flipped operators, $\mathcal{C}'_{9,10}$, gives qualitatively very similar results¹³.

4 Binning performance

To estimate the uncertainties of the OPE prediction, for a given binning, we use the ratios

$$\epsilon_i = \frac{\int_{bin} \rho_i^{KS}(q^2) dq^2}{\int_{bin} \rho_i^{OPE}(q^2) dq^2}, \quad i = 1, 2, \quad \epsilon_{12} = \frac{\int_{bin} \rho_2^{KS}(q^2) dq^2}{\int_{bin} \rho_2^{OPE}(q^2) dq^2} \cdot \frac{\int_{bin} \rho_1^{OPE}(q^2) dq^2}{\int_{bin} \rho_1^{KS}(q^2) dq^2}, \quad (11)$$

where

$$\rho_1(q^2) \equiv \frac{1}{2}(|C^R(q^2)|^2 + |C^L(q^2)|^2) = \left| \mathcal{C}_9^{\text{eff}}(q^2) + \kappa \frac{2m_b m_B}{q^2} \mathcal{C}_7^{\text{eff}}(q^2) \right|^2 + |\mathcal{C}_{10}|^2, \quad (12)$$

$$\rho_2(q^2) \equiv \frac{1}{4}(|C^R(q^2)|^2 - |C^L(q^2)|^2) = \text{Re} \left[\left(\mathcal{C}_9^{\text{eff}}(q^2) + \kappa \frac{2m_b m_B}{q^2} \mathcal{C}_7^{\text{eff}}(q^2) \right) \mathcal{C}_{10}^* \right], \quad (13)$$

are the short-distance factors at high q^2 . They have to be evaluated with the respective effective coefficient $\mathcal{C}_9^{\text{eff}}(q^2)$, Eq. (6) for the KS-model and Eq. (4) for the OPE. The closer ϵ_k to one, the better the performance of the OPE. We calculate the ϵ_k model-independently, *i.e.*, within the global fit, within the 1σ ranges of Figure 4 and corresponding $\mathcal{C}_{9,10}$ values. The outcome is shown in Table 1. As expected, a larger bin interval and one closer to the kinematic endpoint is best. The bins with the best performance are presently [17 – 19] and [18 – 19] GeV^2 , both near the endpoint, followed by the full one [15 – 19] GeV^2 . The deviations $|\epsilon_k - 1|$ from the OPE also include uncertainties within the local charm model. Therefore, improved understanding of the resonance parameters can reduce the uncertainty on the OPE's performance. Such information requires measurements in bins that do resolve the wiggles.

5 Conclusions

The high- q^2 region in semileptonic rare $|\Delta b| = |\Delta s| = 1$ decays is inhabited by wider charm resonances. Using a local model against the OPE provides a data-driven method to test the binning and limitations of the OPE. The ϵ_k ratios defined in Eq. (11) provide data-extracted upper limits on the OPE's binning-related uncertainty, and are useful to identify the most suitable binning. The two bins near the kinematic endpoint perform best, see Table 1. Besides precision studies in these bins measurements in finer q^2 -bins are desirable to improve the local description of resonances. $B \rightarrow K^* \mu \mu$ observables at low recoil are presently consistent with the SM, however, large BSM effects are also allowed. We look forward to future data.

Acknowledgments

GH is happy to thank her collaborators¹³ and the organizers of this inspiring conference for providing an opportunity to speak. The work reported here has been supported in part by the Bundesministerium für Bildung und Forschung (BMBF).

References

1. T. Blake, T. Gershon and G. Hiller, *Ann. Rev. Nucl. Part. Sci.* **65**, 113 (2015) doi:10.1146/annurev-nucl-102014-022231 [arXiv:1501.03309 [hep-ex]].
2. V. Khachatryan *et al.* [CMS Collaboration], arXiv:1507.08126 [hep-ex].
3. R. Aaij *et al.* [LHCb Collaboration], *JHEP* **1602**, 104 (2016) doi:10.1007/JHEP02(2016)104 [arXiv:1512.04442 [hep-ex]].
4. Talk by K. Petridis for the LHCb collaboration at the BEAUTY 2016 conference, May 2-6, 2016, Marseille. LHCb-PAPER-2016-012.
5. T. Aushev *et al.*, arXiv:1002.5012 [hep-ex].
6. B. Grinstein and D. Pirjol, *Phys. Rev. D* **70** (2004) 114005 [hep-ph/0404250].
7. C. Bobeth, G. Hiller and D. van Dyk, *JHEP* **1007** (2010) 098 [arXiv:1006.5013 [hep-ph]].
8. M. Beylich, G. Buchalla and T. Feldmann, *Eur. Phys. J. C* **71** (2011) 1635 [arXiv:1101.5118 [hep-ph]].
9. A. Ali, P. Ball, L. T. Handoko and G. Hiller, *Phys. Rev. D* **61**, 074024 (2000) doi:10.1103/PhysRevD.61.074024 [hep-ph/9910221].
10. F. Krüger and L. M. Sehgal, *Phys. Lett. B* **380** (1996) 199 [hep-ph/9603237].
11. R. R. Horgan, Z. Liu, S. Meinel and M. Wingate, *Phys. Rev. D* **89** (2014) 9, 094501 [arXiv:1310.3722 [hep-lat]].
12. M. Ablikim *et al.* [BES Collaboration], *eConf C* **070805** (2007) 02 [*Phys. Lett. B* **660** (2008) 315] [arXiv:0705.4500 [hep-ex]].
13. S. Braß, I. Nisandzic and G. Hiller, DO-TH 16/06, arXiv:1606.00775 [hep-ph].
14. G. Hiller and R. Zwicky, *JHEP* **1403**, 042 (2014) doi:10.1007/JHEP03(2014)042 [arXiv:1312.1923 [hep-ph]].
15. J. Lyon and R. Zwicky, arXiv:1406.0566 [hep-ph].
16. M. Diehl and G. Hiller, *JHEP* **0106**, 067 (2001) doi:10.1088/1126-6708/2001/06/067 [hep-ph/0105194].
17. S. Descotes-Genon, L. Hofer, J. Matias and J. Virto, arXiv:1510.04239 [hep-ph].